Diffusion-Based Single Particle Sizing Method Provides Precise Measurement of Nanoparticle Individual Size Variation and Formation of Bioconjugates

by

Ardalan Ardeshiri

Presented to the Division of Biomedical Engineering within
The Department of Science & Engineering
and the Oregon Health & Science University
School of Medicine
in partial fulfillment of
the requirements for the degree of
Master of Science
in
Biomedical Engineering

December 2009

Department of Science & Engineering
School of Medicine
Oregon Health & Science University

Certificate of Approval

This is to certify that the Master's thesis of
Ardalan Ardeshiri
has been approved

_____
Dr. Tania Q. Vu, Thesis Advisor
Assistant Professor

_____
Dr. Steven L. Jacques
Professor

_____
Dr. Nabil J. Alkayed
Professor

ACKNOWLEDGMENTS

This work was done in the laboratory of Dr. Tania Vu at Oregon Health Science University. I am grateful to Dr. Vu for giving me the opportunity and providing the resources to do this work.

I would like to thank all of the members of the Vu lab, present and past, for their help and assistance throughout my time at Oregon Health Science University.

Also, I would like to thank my committee members, Steve Jacques and Nabil Alkayed for their willingness to participate on this committee and their time. In addition, I'd like to thank William Roberts for his insight and continual support. Finally, I would like to thank my parents and my sister for all their love and encouragement throughout my time at OHSU.

This study was supported by a DOD grant to Dr. Tania Vu.

TABLE OF CONTENTS

LIST OF FIGURES

ABSTRACT

Diffusion-Based Single Particle Sizing Method Provides Precise Measurement Of Nanoparticle Individual Size Variation and Formation of Bioconjugates.

Ardalan Ardeshiri B.S.

Master's Thesis
Division of Biomedical Engineering within
The Department of Science & Engineering
and the Oregon Health & Science University
School of Medicine

December 2009
Thesis Advisor: Tania Q. Vu

We report an approach, diffusion based single particle sizing (DBSPS), to determine hydrodynamic size distributions of fluorescent nanoparticle quantum dots (QDs) and QD bioconjugates. We used fluorescence video-microscopy for determination of fluorescent particle trajectories in solution. The trajectories provide spatial and temporal information required for the determination of the diffusion coefficients (D) through mean square displacement (MSD) analysis. Subsequently, the hydrodynamic radii (R_h) of the individual particles were estimated using the Stoke-Einstein formula. DBSPS measures hydrodynamic size of single particles, rather then ensemble measurements. This allows the tracking and analysis of small single particles even when they are present in heterogeneous samples containing larger particles. Our results demonstrate that DBSPS accurately measures hydrodynamic dimensions of QD bioconjugates and pre-calibrated fluorescent polystyrene nanospheres, provides a measure of QD-biomolecule conjugation efficiency and identifies and excludes QD aggregates (multiple QD complexes). Researchers who design QD bioconjugates for aqueous settings can obtain highly tuned QD bioconjugate hydrodynamic size distributions using DBSPS.

1. Introduction and Literature Review

1.1 Motivation

A major goal in bionanotechnology is to create nanoparticles and nanoparticle bioconjugates with precise size- and valence- control.[1-4] In practice, however, synthesis is a probabilistic process that results in nanoparticles of varying size and varying numbers of bound bioconjugates.[5] Moreover, after synthesis, the effects of temperature, time, and exposure to solutions of varying compositions introduce additional factors that may contribute to variation in the size distribution of individual nanoparticle bioconjugates in any single batch of nanoparticle conjugates.[6] In order to synthesize nanoparticle bioconjugates of known size, accurate and sensitive methods are needed to evaluate the size distribution of samples of nanoparticle bioconjugates in solution.

1.2 Existing Methods For Measuring Nanoparticle Size

Currently, a number of different methods are used to measure the size of nanoparticle bioconjugates, but to our knowledge, no reliable method has been established to quantitatively assess the hydrodynamic size variations of individual nanoparticle bioconjugates. Gel electrophoresis, size-exclusion chromatography (SEC)[7-9], atomic force microscopy[9] and ultracentrifugation[10, 11] are current nanoparticle-sizing techniques of choice. However, a major deficit in these methods is that they yield averaged information (e.g. average band fluorescence or peak signal) rather than information about individual size variations within a sample.[12-14] As a result, it is not possible to determine if individual particles within a sample contributed equally to the averaged size measured, or if the average size measured has a higher contribution from select subpopulations of particles. A simple technique that would allow investigators to distinguish among these two conditions would be valuable for characterizing nanoparticles sizes.

Classical studies have used Stokes-Einstein to estimate the ensemble average hydrodynamic sizes of spheres, cells, and proteins through photon correlation spectroscopy (PCS, also known as dynamic light scattering (DLS)) or fluorescence correlation spectroscopy (FCS). These PCS/FCS methods are based on the same concept as diffusion-based estimates.[15, 16] However, these methods do not reveal small variations in the sample size because they measure the ensemble average size of the particles in the sample.[17-21] As yet, while early studies have examined these methods as a means to size nanoparticles, diffusion based methods have not yet been systematically examined and demonstrated to be a viable and sensitive technique for routine measurement of individual size variations of nanoparticle bioconjugates.

1.3 Aim of This Study

In the current studies, we investigated if, through the combination of single particle tracking methods and diffusion-based Stokes-Einstein estimations, we could: 1) accurately measure the individual size distribution of both unconjugated and conjugated fluorescent nanoparticles quantum dot (QDs) bioconjugates; and 2) apply this method to provide sensitive confirmation of successful conjugation of monovalent QDs bearing one IgG protein. We find that measurements using Stokes-Einstein estimates from diffusion-based single particle sizing (DBSPT) is especially well-suited and sensitive for sizing nanoparticles with nanometer sensitivity because we of the high sensitivity and accuracy (≈ ± 3 nm) for particles in the nano (as opposed to micro) size regime. DBSPS sensitivity allowed us to accurately measure and differentiate the size distributions of samples containing un-conjugated QDs and QDs bearing biomolecules for two widely-used conjugation systems (1-Ethyl-3-[3-dimethylaminopropyl]-carbodiimide hydrochloride (EDC)[22, 23] and biotin-streptavidin[9, 24-26]). These experiments, describe a two-dimensional single particle tracking method to estimate single QD bio-conjugates hydrodynamic dimensions, and demonstrate that DBSPS is an effective methodology for characterizing QD bio-conjugates.

2. Methods

2.1 QD and Green Fluorescent Nanosphere Sample Preparation

Quantum dots (COOH-QD655, NH-QD655 and streptavidin-QD 655) were purchased from Invitrogen. Green fluorescent polystyrene calibration nanospheres (with radii of 12.5 ± 2.5, 25.5 ± 3.8 and 35.5 ± 5.6 nm) were purchased from Duke Scientific Corporation and used for size calibration. Specific size calibrations of the nanosphere suspensions were performed by photon correlation spectroscopy (PCS) corresponding to the exact lot numbers of the samples obtained from the supplier.

2.2 Synthesis of QD-IgG Bioconjugates

Goat anti-human IgG Fc (Chemicon) was used to make 1-Ethyl-3-[3-dimethylaminopropyl]carbodiimide hydrochloride (EDC) cross-linked QD-IgG and QD-streptavidin-biotin-IgG bioconjugates. To make EDC-activated QD-IgG bioconjugates, EDC (2 µl, 10 mg/ml, Pierce) was added to 80 µl of 1 µM COOH-QD655 solution (in freshly prepared 10 mM borate buffer, pH 7.4) and placed on a shaker at room temperature for 15 min. Excess EDC was removed by filtering (micron, MWC 10 KD, Millipore) the EDC-activated COOH-QD solution x5 for 20 min each at 15,000g in 500 µl of 10 mM borate buffer (pH 7.4). Following, EDC-activated COOH-QDs were resuspended in 82 µl of PBS (pH 7.2). QD-IgG bioconjugates of varying molar ratios were formed at: 1 QD: 0.5 IgG, 1 QD: 1 IgG, 1 QD: 2 IgG, and 1 QD: 4 IgG by combining IgG at: 5.8 ul of 2 mg/ml, 1 mg/ml, 0.5 mg/ml or 0.25 mg/ml, with 20.5 µl of 1 uM EDC-activated COOH-QDs, respectively. The mixtures were placed on a shaker for 1 hr at room temperature. The resulting QD-IgG conjugates were stored at 4°C.

QD-streptavidin-biotin-IgG bioconjugates were made by biotinylating IgG: 8 µl of 2 mg/ml IgG was incubated with 19 µl of 0.1 mg/ml (30-fold excess) NHS-Biotin-PEO (Pierce) overnight at 4°C then dialyzed in 500 ml PBS (pH 7.2) to remove unbound biotin by-product (3 hrs, Slide-A-Lyzer 7 KD MWCO, Pierce).

QD- streptavidin -IgG bioconjugates were formed at varying molar ratios: (1 QD-SA: 1 biotin-IgG, 1 QD-SA: 2 biotin-IgG, 1 QD-SA: 4 biotin-IgG and 1 QD-SA: 8 biotin-IgG) by combining biotinylated-IgG:10 µl of 0.1 µM, 0.2 µM, 0.4 µM or 0.8 µM to 10 µl of 0.1 µM QD-SA, respectively. The mixture was incubated at 4°C for 1 hr for conjugation to occur.

2.3 Single Particle Measurements

The imaging chamber consisted of a 35 mm Petri dish, with a 5 mm diameter hole in the center; the bottom was glued to a glass coverslip (Fisher Scientific). This created a small chamber, ≈ 50 µl in volume, in the center of the Petri dish. Green fluorescent polystyrene nanospheres were sonicated (Branson 2510) for 15 s at the lowest setting to disperse aggregates. To load the sample solution in the imaging chamber, 50 µl of the 20 pM sample solution in PBS (QDs and polystyrene nanospheres) was pipetted into the imaging chamber. The top of the imaging chamber was then covered with a coverslip (Fisher Scientific) to close the chamber. To allow the sample solution to reach steady state temperature, video acquisition was begun 10 min after sample loading. The ambient temperature of the imaging chamber was measured before and after imaging with a thermocouple applied to the coverslip (Fisher Scientific).

2.4 Real Time Video Microscopy

To obtain real time videos of sample solutions containing QDs or green fluorescent-loaded nanospheres, a high magnification objective (x100, NA: 1.4) was focused on the sample solution at a distance approximately 0.8 um above the bottom of the chamber. Each measurement session consisted of recording 10 videos of 25 s duration at a 31 ms/frame integration time (512 x 512 pixels, 0.19 µm/pixel, 3 x 3 pixel binning). Images were acquired using a fluorescent microscope (Zeiss, Axiovert) equipped with excitation and emission filters (Chroma), and a cooled monochrome CCD camera (Axiocam). Image acquisition and processing were performed using AxioVision 4.4 software (Zeiss) and ImageJ 1.38X (NIH).

2.5 Two-Dimensional Particle Tracking Analysis

Depending on particle size, fluorescent QDs and nanospheres were monitored and tracked over 5-214 frames (particle positions) with an average of 9.7 ± 6.6 frames (n= 3465 particle trajectories). The total number of frames acquired is limited by movement of particles out of the focal Z-plane due to diffusion.[27-29] A trajectory was assigned for each detected fluorescent particle using ImageJ 1.38X (NIH) with the particle tracking plugin (written by Guy Levy at the computational biophysics lab, ETH Zurich).[30] Each individual trajectory was visually checked, frame by frame, to make sure that the tracking was done correctly for each particle; we discarded trajectories that were incorrectly assigned because of interference from multiple particles or incorrect position assignments. The two-dimensional (2D) mean square displacement (MSD), the squared distance that a particle moves over to the time elapsed, of each trajectory was calculated using the following equation[31-33]:

$$MSD_{n\Delta t} = \left\langle r^2_{xy} \right\rangle = \frac{1}{N-n} \sum_{i=1}^{N-n} [(x_{i+n} - x_i)^2 + (y_{i+n} - y_i)^2] \qquad (1)$$

Where r is particle displacement between subsequent frames, x_i and y_i are the particle coordinates on frame i, N is the total number of frames (independent particle position samples) in the trajectory, Δt is the time between frames, n is the total number of time steps over which the MSD is calculated and $n\Delta t$ is the time interval over which the MSD is calculated.

To estimate the particle diffusion coefficient (D) we use 2D particle tracking. 2D tracking is appropriate for DBSPS even tough our particle has three degrees of freedom in motion. The proof for this is the following: the three-Dimensional (3D) walk is expressed as the distance (r) from the origin (x=0,y=0,z=0) where diffusion first began. The squared distance r^2 is related to the position of the particle along the x, y and z axes after N steps:

$$r^2 = \left(\sum_{i=1}^{N} x_i\right)^2 + \left(\sum_{i=1}^{N} y_i\right)^2 + \left(\sum_{i=1}^{N} z_i\right)^2 \qquad (2)$$

But the movements in the x, y and z direction are basically equivalent, hence upon sampling many such particle trajectories, the net average value $\langle r^2 \rangle$ after N steps is:

$$\langle r^2 \rangle \approx 3\left(\sum_{i=1}^{N} x_i\right)^2 \qquad (3)$$

Similarly, the 2D random walk is represented by the distance (r_{xy}) from the origin in the xy plane:

$$r_{xy}^2 = \left(\sum_i x_i\right)^2 + \left(\sum_i y_i\right)^2 \qquad (4)$$

which can be restated as

$$\langle r_{xy}^2 \rangle \approx 2\left(\sum_{i=1}^{N} x_i\right)^2 \qquad (5)$$

Therefore,

$$\langle r^2 \rangle \approx \frac{3}{2}\langle r_{xy}^2 \rangle \qquad (6)$$

In other words, one can observe $\langle r^2_{xy} \rangle$ using a camera to observe many particle random walks, and convert the data to $\langle r^2 \rangle$, which is related to the *D*:

$$\frac{\partial \langle r^2 \rangle}{\partial N} \approx 6D \qquad (7)$$

or alternatively,

$$\frac{\partial\langle r_{xy}^2\rangle}{\partial N} \approx \frac{2}{3}6D = 4D \qquad (8)$$

To minimize the error in our diffusion coefficient estimation, only the first two points in the 2D MSD function (see DBSPS error analysis) were fitted to the relation for a 2D random walk:[34]

$$\textit{MSD-slope}_{\textit{(between first two points)}} \approx \frac{\partial\langle r^2{}_{xy}\rangle}{\partial N} = 4D \qquad (9)$$

Where *D* is the diffusion coefficient. Using the estimated *D*, the hydrodynamic radius (R_h) of each single particle can be estimated using Stokes-Einstein equation:

$$R_h = \frac{K_B T}{6\pi\eta D} \qquad (10)$$

Where R_h is the hydrodynamic radius, K_B is the Boltzmann constant, *T* is the absolute temperature and η is the viscosity. In the R_h estimations, water viscosity (η) was assumed to be 9.11×10^{-4} Pa s (at 24°C) and T = 297 K was used.

2.6 Particle Fluorescence Intensity Analysis

To distinguish single particles from multiple particle complexes a single video frame for each particle was visually selected based on greatest fluorescent intensity. The fluorescent intensity of each particle is subsequently measured using the Axio Vision 4.4 (Zeiss) fluorescence intensity (grey scale) measuring application. A set number of pixels were predetermined for all images to standardize the analysis. Significant statistical difference in fluorescence intensity across particles was tested by paired t-test ($P < 0.05$).

2.7 DBSPS Error Analysis

DBSPS's accuracy depends on the accuracy of the particle tracking[27], sample temperature/viscosity fluctuation and shape of particles measured. The accuracy of particle tracking (ImageJ particle tracking software) is based on two factors: the number of independent particle positions samples captured and particle position assignments.

The error contributed from the limited amount of independent position samples is the limiting factor in DBSPS sensitivity; it requires calculation of stochastic uncertainty. The stochastic uncertainty is described by equations derived by Qian et al (1991). Qian and colleagues showed that there is a relative stochastic uncertainty in estimating the MSD vs. time slope, and this uncertainty propagates to the estimation of the diffusion coefficient:

$$\sigma_D = \pm\sqrt{\frac{2m}{3(N-m)}} \qquad (11)$$

Where σ_D is the relative stochastic uncertainty in the diffusion coefficient, *m* is the last MSD point used to estimate the MSD slope, and *N* is the total number of particle position measurements. The MSD slope can be estimated at any point within the MSD-time interval[34]. Within the limits of the accuracy of the experimental measurements of particle position (discussed below), the variance decreases with an increasing number of single particle position measurements and increases with increasing *m* because the larger the *m* the smaller the number of statistically independent samples of displacement within the interval $N\Delta t$. Hence, one way to decrease statistical variance is to derive the MSD slope between the first MSD point (zero) and the second MSD point where m=1, maximizing the number of independent samples within the interval $N\Delta t$. Applying the stochastic uncertainty calculations to our data (see Results) shows that we obtain ≈ ± 30% in estimating single particle $R_{h.}$ However, this relative error from stochastic uncertainty translates into an absolute error of only ≈ ± 3 nm for 10 nm particles (QD size range). DBSPS sensitivity is, therefore, approximately 3 nm for QDs.

The error in particle position assignment is another error to be considered. The error in ImageJ particle position assignments is approximately 0.2 pixels[30] or 38 nm (190 nm pixels size x 0.2 = 38 nm). In order to evaluate how the position assignment error affects our size measurements, it has to be compared to the particle displacement in each step of the trajectory (average: 1.52 μm for QDs). This comparison yields a 2.5 % (0.038 μm / 1.52 μm) error in position assignment. The 2.5 % error in position assignment is negligible compared to the error due to the limited number of independent position samples (≈ ± 30%). [34, 35]

Another factor affecting DBSPS accuracy is fluctuation in the sample solution's temperature/viscosity. We noted an increase in the sample solution temperature: 0.26 ± 0.05 °C per 25 s imaging (UV exposure). An increase of 0.26 °C decreases the solution viscosity and results in a ≈ ± 0.07 nm error in QD R_h. However, this error is within the stochastic uncertainty (≈ ± 3 nm) and smaller then the DBSPS threshold of sensitivity. Therefore, the error from temperature/viscosity fluctuation will be within the experimental noise and not influence DBSPS measurements significantly.

Moreover, the Stoke-Einstein formula is most accurate for spherical particles. As a result, shapes of particles that are different from spheres may also be a source of error. However, this source of error is considered negligible for particles with length-to-diameter ratios (L/D) of less then 7.2,[36] which form an effective spherical shape due to rotational diffusion.[36-40] The hard (inorganic) core of 655 QDs, as determined by TEM, have a L/D ratio of 1.2-2.0.[41] For QD bio-conjugates (e.g. QDs coated with a saturated layer of 20 kDa PEG molecules) the effective thickness of the organic shell is about 10.8 ± 3.3 nm.[14] Since the inorganic cores of 655 QDs are about 9 nm in radius as measured with TEM (reported by Invitrogen), an additional organic layer (10.8 nm) will still exhibit a L/D ratios smaller then 7.2. Therefore, QD and QD-bioconjugates in solution should form an effective spherical shape due to rotational diffusion and the error contribution to DBSPS from the shape of the QDs should be negligible.

Finally, because the objective lens has a high numerical aperture (1.4), it may only view particles that remain with a limited z-plane of focus (z-plane width

≈ 300 nm). Consequently, longer steps could move the particle out of the focal plane, such that the particle is not detected. Meanwhile, smaller steps more easily remain within the focal plane. This bias due to the limited z-plane of focus causes an underestimate of the number of larger step-sizes taken by the particle and, therefore, also causes an underestimate of the diffusion coefficient. However, this bias does not exist if particle step-size is much smaller then the z-plane of focus. Even tough the observed mean QD step-size is 1.52 μm (observed QD step-size depends on the camera acquisition rate, we used a 31 ms/ frame camera) the real QD step-size is much smaller. The real QD step-size is about 10 nm (particle step-size is in the same size range as particle size[49]) and much smaller then the z-plane of focus (≈ 300 nm). Therefore, the limited z-plane of focus does not effect QD size measurements.

3. Results

3.1 QD Diffusion Analysis

Determination of the hydrodynamic radius (R_h) using DBSPS relies on accurate acquisition of single particle trajectories[42]. Particle trajectory acquisition within the xy plane is determined by fluorescence video-microscopy. Figure 1 illustrates the steps involved in estimating the R_h of single QD's or QD bio-conjugates using DBSPS. Figure 1A is a representative video frame showing trajectories of multiple QD's. For a single QD trajectory (Fig. 1B), the mean squared displacement (MSD) plot (Fig. 1C) exhibits a linear relationship, indicating QD Brownian motion in solution.[34, 43] To minimize the stochastic uncertainty in R_h estimation, the slope of the MSD plot was obtained between the first two MSD points (see Methods, DBSPS error analysis). The slope is proportional to four times the diffusion coefficient[34, 43] (Fig. 1D). The R_h of each individual particle is computed with the Stoke-Einstein formula (Fig. 1D), which inversely relates the hydrodynamic size of spherical particles to their diffusion coefficients.

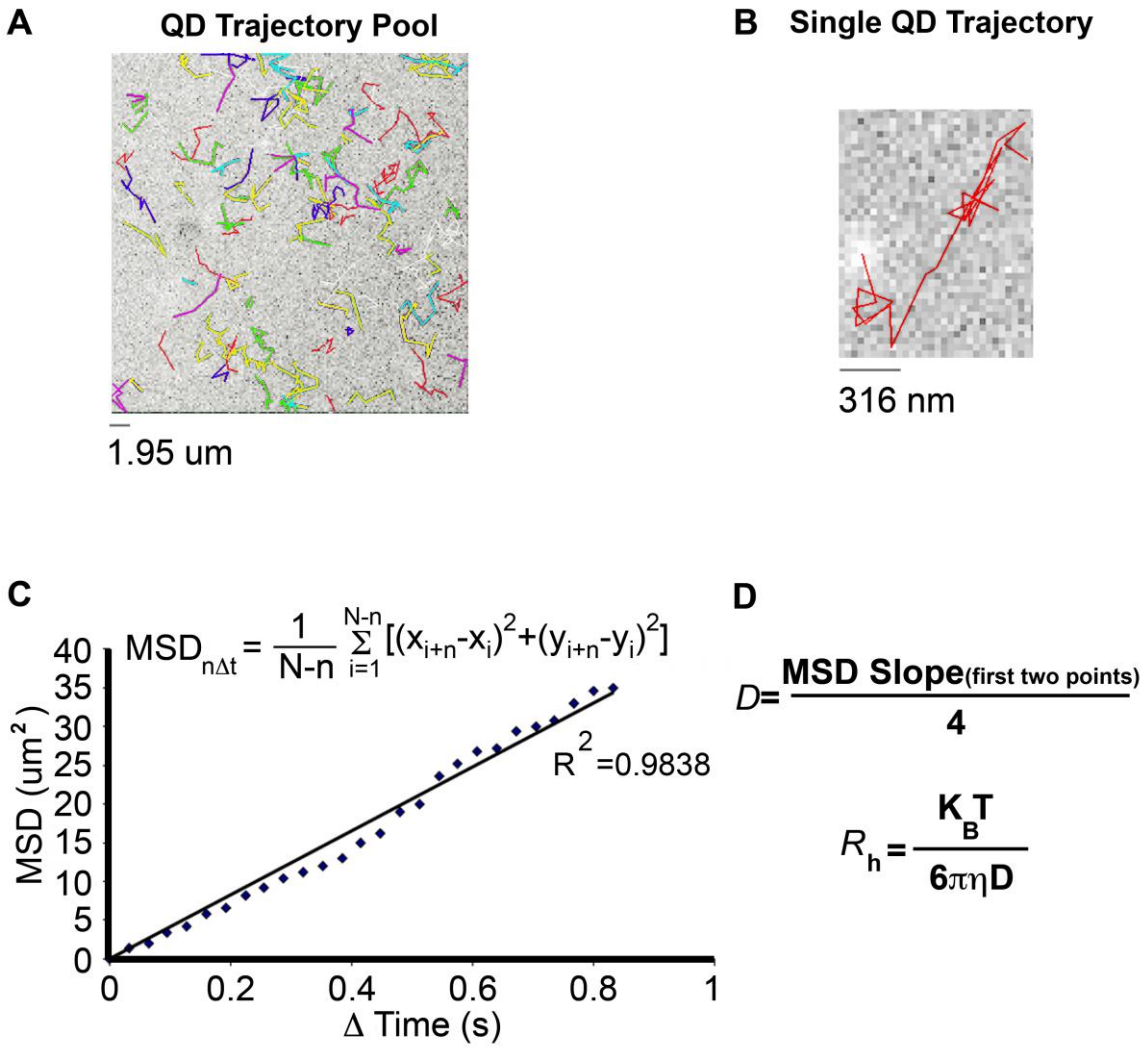

Figure1. A schematic representation of DBSPS-based size determination. (A) Fluorescent nano-particles diffusing in water are imaged with a camera attached to a fluorescent microscope. Trajectories for each particle are determined via Image J particle tracking software. (B) A close-up of a single streptavidin QD 655 trajectory that appears to be randomly diffusing in water. (C) A linear plot of mean square displacement (MSD) of the streptavidin QD 655 in panel B indicating random diffusion. (D) The slope of the MSD between the first two points is divided by four to obtain the diffusion coefficient and the Stoke-Einstein equation is used to calculate hydrodynamic radius from the diffusion coefficient.

3.2 Polystyrene Nanospheres

The accuracy of DBSPS was tested partly by measuring the hydrodynamic radii of uniform, pre-calibrated polystyrene nanospheres containing green fluorescent dye. These commercially-synthesized nanospheres are suitable as calibration spheres because they possess well-controlled dimensions whose average size has been measured using photon correlation spectroscopy (PCS). Figure 2 shows that the DBSPS-measured sizes closely correspond in value to those measured by the manufacturer through PCS. DBSPS measurements of nanospheres supplied as R_h of 12.5 ± 2.5 nm, 25.5 ± 3.8 nm and 35.5 ± 5.6 nm showed Gaussian-shaped distributions with average sizes of 10.6 ± 2.5 nm, 23.5 ± 5.6 nm and 38.4 ± 8.5 nm, respectively (Fig. 2A-C, asterisk). The spread of each Gaussian distribution represents both the variability in the actual sizes of the nanospheres as well as the variance inherent in DBSPS due to stochastic uncertainty (red horizontal bar). These results show that the DBSPS measurements of the average sizes of calibrated nanospheres closely reflect those of PCS measurements for three separate calibrated nanosphere sizes. This correspondence between DBSPS and PCS measurements attests to the accuracy of DBSPS.

The error inherent in DBSPS measurements is due to the stochastic nature of MSD analysis. All single particle DBSPS R_h estimations are therefore shown with the stochastic uncertainty (Figs. 2, 4-6, red horizontal bars). The variance within the stochastic uncertainty represents the error inherent in DBSPS. However, the variance outside of the stochastic uncertainty represents variability in the actual size of the particles. Our results show that DBSPS obtains 9.7 ± 6.6 independent particle positions (n= 3465 particle trajectories). Therefore, the stochastic uncertainty in R_h estimation is approximately ± 30% (see Methods, DBSPS error analysis). An error of 30% translates into an absolute uncertainty of only a few nanometers for nano-particles (≈ ± 3 nm for 10 nm particles). This small uncertainty in R_h at the nano-scale indicates that DBSPS is suited for nano-particle QDs.

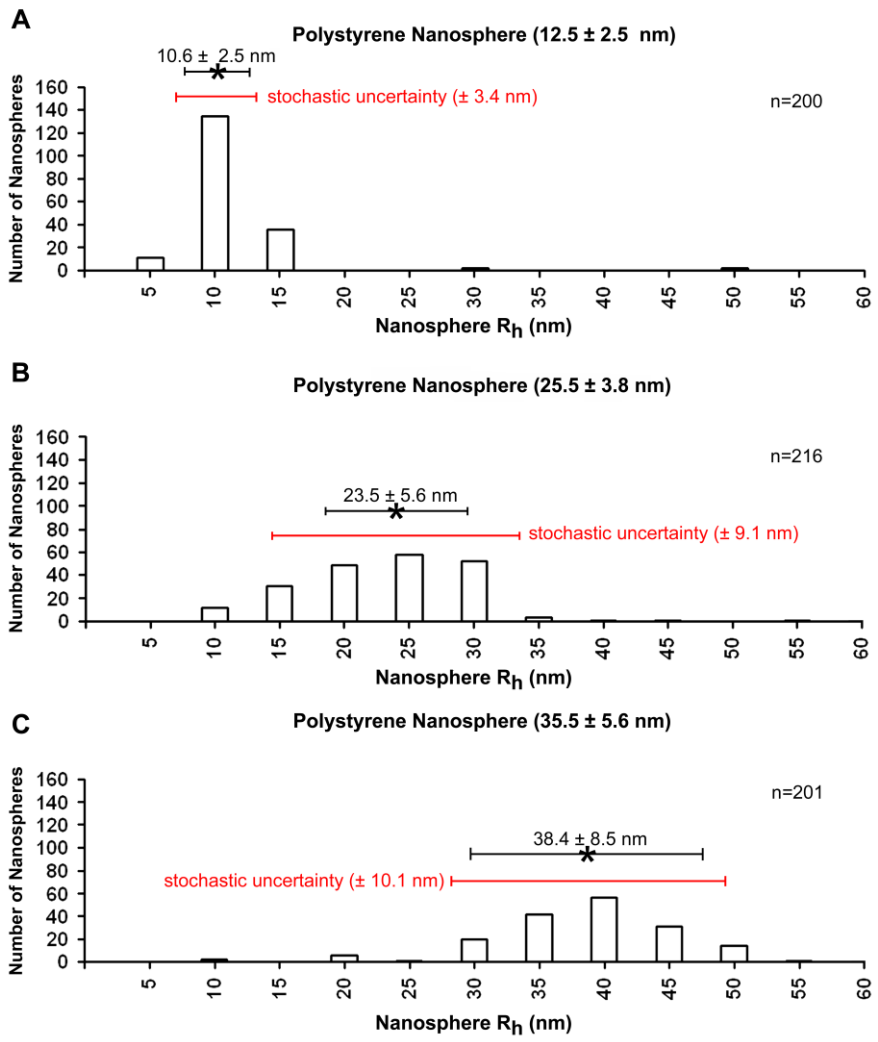

Figure 2. DBSPS R_h measurements of polystyrene nanosphres (Duke scientific) showed that DBDPS measures hydrodynamic dimensions within a few nanometers of PCS measurements reported by the manufacturer. (A-C) DBSPS R_h measurements on three nanospheres with PCS measurements of (mean ± SD) 12.5 ± 2.5 nm, 25.5 ± 3.8 nm and 35.5 ± 5.6 nm R_h yield DBSPS measurements of 10.6 ± 2.5 nm, 23.5 ± 5.6 nm and 38.4 ± 8.5 nm R_h, respectively. The Error due to stochastic uncertainty (red horizontal bar) was calculated for all particle trajectories. Histogram bin size: 5nm

3.3 Measurements of QDs With Different Organic Coatings

DBSPS R_h measurements of COOH QD 655 (coated with carboxyl groups), NH QD 655 (modified by the conjugation of multiple PEG molecules) and streptavidin QD 655 (with additional streptavidin proteins conjugated onto the PEG shell) yielded, 11.5 ± 3.2 nm, 15.3 ± 9.7 nm and 19.6 ± 9.2 nm, respectively (Fig. 3A-C, asterisk). These DBSPS measurements are a few nanometers larger then the radii reported by the manufacturer, 9 nm for COOH QD 655 as measured with TEM, 10 nm for NH QD 655 as measured with TEM and 11-14 nm for streptavidin QD 655 as measured with SEC. TEM and SEC measurements are smaller then DBSPS measurements. The differences are expected because TEM can't measure the QD organic coating as well as the extra hydrodynamic dimension, and SEC measures the QD ensemble average size based on protein standards.[14] SEC protein standards underestimate QD size because proteins in the chromatography column compress to a smaller size.[44] Note that the variance in NH and streptavidin QD 655 R_h measurements are greater then the variance in COOH QD 655 R_h measurements. Since each NH and streptavidin QD particle may contain varying number of PEG/streptavidin molecules, the large variance observed in these QDs is most likely due to varying number of PEG/streptavidn molecules coating the QDs. These results indicate that DBSPS is accurately measuring QD R_h.

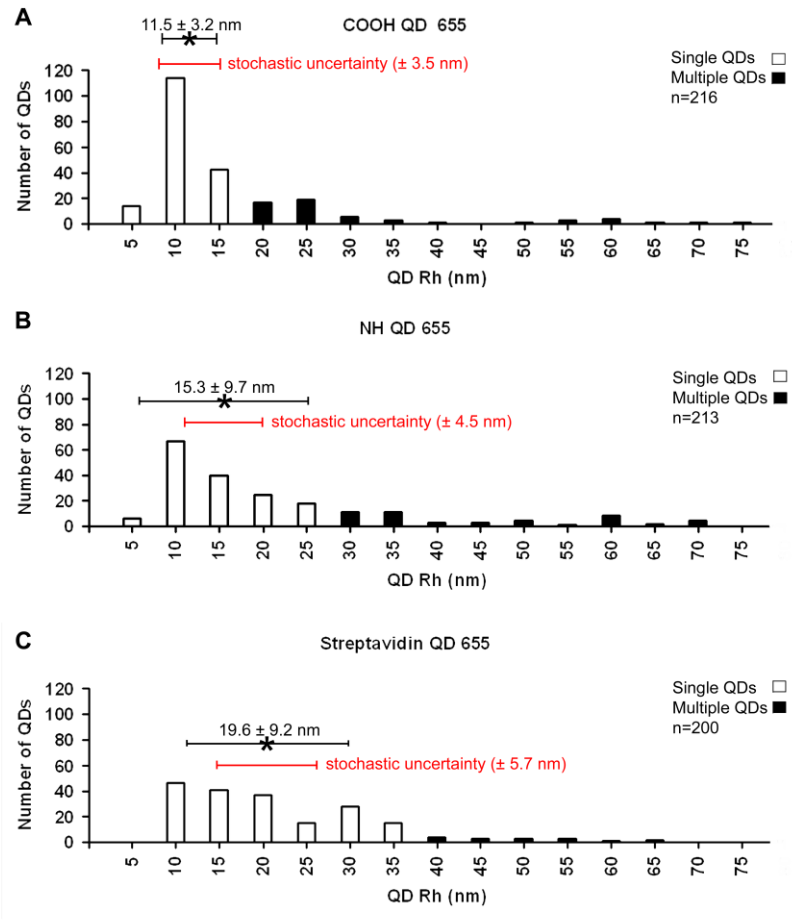

Figure 3. DBSPS R_h measurements of three different functionalized Invitrogen QDs showed that larger organic coatings yield larger QD R_h as measured by DBSPS and the measurements are in the same range as measurements made by TEM and SEC. (A-C) DBSPS R_h measurements for the COOH QD 655, NH QD 655 and streptavidin QD 655 yield an Rh of (mean ± SD) 11.5 ± 3.2 nm, 15.3 ± 9.7 nm and 19.6 ± 9.2 nm, respectively. DBSPS and QD fluorescence intensity analysis (Fig. 4) differentiates single QDs (white bars) and multiple QDs (black bars). The Error due to stochastic uncertainty (red horizontal bar) was calculated for all particle trajectories. Histogram bin size: 5nm.

3.4 Identifying Multiple QD Complexes

QD solutions sometimes contain multiple QD complexes. For single particle measurements one needs to identify and differentiate multiple QD complexes from single QDs. These complexes can be differentiated using DBSPS in combination with fluorescence intensity (grey scale units) measurements, analyzed quantitatively with Axiocam imaging software (Zeiss). Fluorescence intensities of all QDs, with R_h measured with DBSPS, were analyzed with Zeiss Axiocam software (Fig. 4). Differences between fluorescence intensity distributions were tested for statistical significance ($P<0.05$) with paired t-tests. QDs measured with DBSPS, having R_h values close to those reported for single QDs, hold lower fluorescence intensities than QDs with larger R_h values. Brighter fluorescence is expected for multiple QD complexes.[45] Figure 4 shows the fluorescence intensity measurements for all COOH QD 655s, NH QD 655s and streptavidin QD 655s measured with DBSPS. Compared to intensities of particles with smaller R_h values, we found significantly ($P<0.05$) brighter fluorescence intensity for QDs at $R_h \geq 20$ nm (COOH QD 655) , $R_h \geq 30$ nm (NH QD 655) and $R_h \geq 40$ nm (streptavidin QD 655) (Fig. 4A-C). These results suggest that COOH QD 655 multiple QD complexes have $R_h \geq 20$ nm, NH QD 655 multiple QDs have $R_h \geq 30$ nm and streptavidin QD 655 multiple QD complexes have $R_h \geq 40$ nm. Moreover, these data suggest that single NH QD 655s are larger then COOH QD 655s and single streptavidin QD 655s are larger then both COOH QD 655s and NH QD 655s. We, therefore, conclude that DBSPS-captured images permit the exclusion of multiple QD complexes from those of single QDs through fluorescence intensity analysis. Such analysis is essential in QD bio-conjugate characterization because QD bio-conjugates sometimes form multiple QD complexes due to the conjugation process.[23]

In summary, Figs. 3 & 4 show that DBSPS is sensitive to size differences due to different organic coatings and DBSPS measurements are within few nanometers of values measured by other methods (TEM and SEC). Also, DBSPS in combination with fluorescence intensity analysis yields average R_h values that exclude multiple QD complexes (black bars) from single QDs (white

bars). These measurements provide a more precise single QD average size measurements compared to ensemble size measurements, which can’t exclude multiple QD complexes.

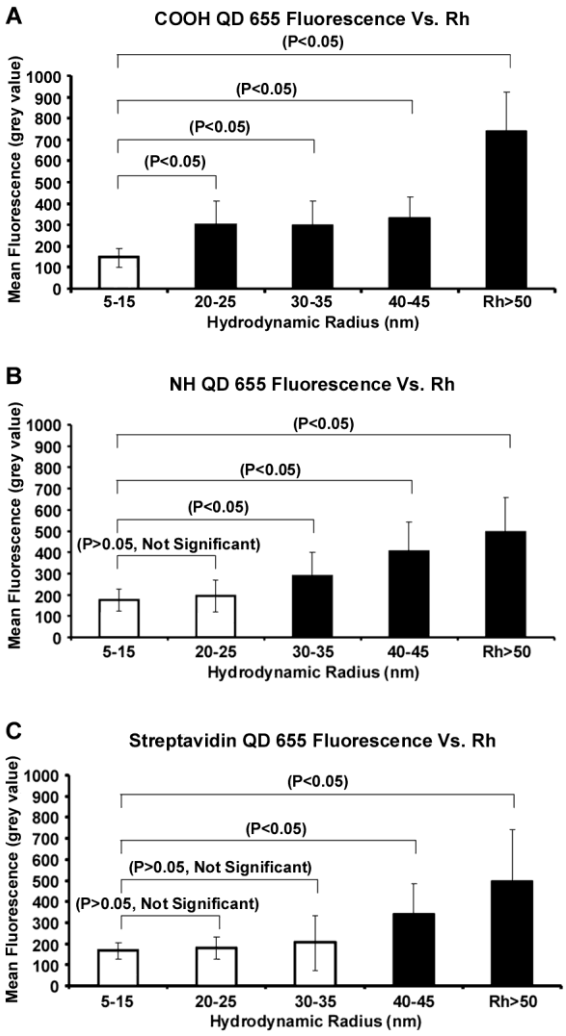

Figure 4. DBSPS in combination with fluorescence intensity analysis of QD complexes differentiates between single and multiple QDs. QD fluorescence intensities were correlated to DBSPS measurement and we show that (A) COOH QD 655 QDs (n= 216) measured with DBSPS at $R_h \geq 20$ nm (black bars) show significantly ($P<0.05$, paired t-test) brighter fluorescence intensity compared to COOH QDs measured at 5-15 nm R_h (white bars). (B) NH QD 655 QDs (n=213) measured with DBSPS at $R_h \geq 30$ nm show significantly ($P<0.05$, paired t-test) brighter fluorescence intensity compared to NH QDs measured at 5-25 nm R_h. (C) Streptavidin QD 655 QDs (n= 200) measured with DBSPS at $R_h \geq 40$ nm show significantly ($P<0.05$, paired t-test) larger fluorescence intensity compared to streptavidin QD 655s measured at 5-35 nm R_h.

3.5 EDC-mediated COOH QD 655-IgG Conjugates

The size properties of COOH QD 655 and EDC-mediated COOH QD 655-IgG conjugates were characterized with DBSPS to see if DBSPS detects stoichiometry-dependent size changes. Three separate experiments demonstrated (Fig. 5) that, depending on the conjugation ratio, the COOH QD 655-IgG conjugates are ≈ 17-27 nm (R_h) larger then un-conjugated COOH QD 655s. Therefore, our results clearly distinguish un-conjugated from conjugated QDs. Also, DBSPS provides a measure of the conjugation efficiency. For example, DBSPS shows that EDC mediated QD-IgG conjugation shows 88 % conjugation efficiency (12 % of QDs remain at the un-conjugated COOH QD 655 size range, 11.5 ± 3.2 nm).

As a control, COOH QD 655s were subjected to EDC treatment without exposure to IgG. The control sample showed an R_h of 11.7 ± 2.6 nm (Fig. 5A, asterisk), similar to COOH QD 655 not activated with EDC (11.5 ± 3.2 nm), but EDC-activated control samples contained more multiple QD complexes (black bars, differentiated by fluorescence intensity analysis, data not shown). IgG exposure to EDC-activated QDs, however, caused a significant increase in single QD R_h values compared to control. These results show that, compared to control, QD-IgG conjugates at increasing QD:IgG binding ratios of 1:0.5, 1:1, 1:2 and 1:4 yielded significantly larger R_h values of 28.8 ± 11.5 nm, 30.9 ± 12.9 nm, 35.4 ± 10.8 nm and 38.5 ± 12.2 nm, respectively (Fig. 5B-E, asterisk). These results clearly show an increase in size with increasing QD:IgG binding ratios. The R_h histograms also elucidate the QD-IgG conjugation efficiency (88 %) achieved with EDC mediated conjugation. This information is useful when comparing different conjugation schemes.

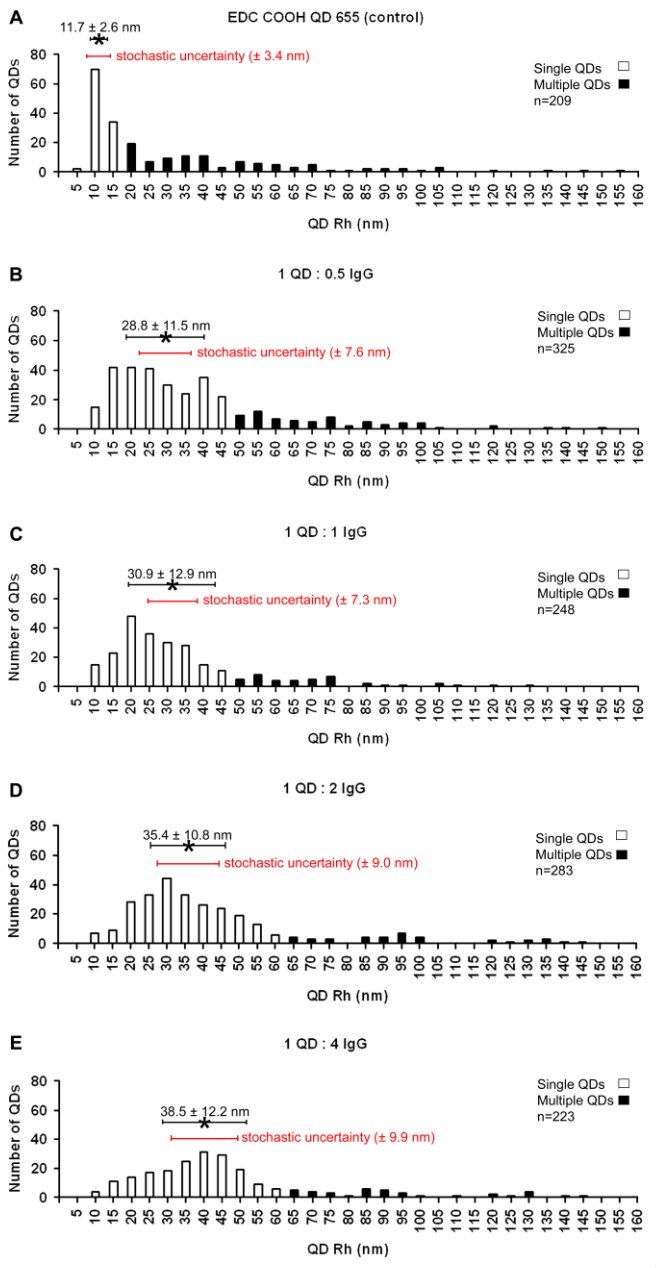

Figure 5. DBSPS measurements showed that, depending on the conjugation ratio, EDC mediated COOH QD 655-IgG conjugates are 17-27 nm (R_h) larger compared to control. (A) QD 655 COOH control sample that were subjected to EDC treatment with out exposure to IgG yielded an R_h of (mean ± SD) 11.7 ± 2.6 nm. (B-E) QD-IgG conjugates at increasing QD:IgG binding ratios of 1:0.5, 1:1, 1:2 and 1:4 measure significantly larger R_h of 28.8 ± 11.5 nm, 30.9 ± 12.9 nm, 35.4 ± 10.8 nm and 38.5 ± 12.2 nm, respectively. DBSPS and QD fluorescence intensity analysis differentiates single QDs (white bars) and multiple QDs (black bars). The Error due to stochastic uncertainty (red horizontal bar) was calculated for all the particle trajectories. Histogram bin size: 5nm.

3.6 Streptavidin-Biotin -mediated QD 655-IgG Conjugates

The streptavidin-biotin conjugation system is another often-used conjugation scheme. To see if DBSPS detects a difference between the EDC and streptavidin-biotin QD-IgG conjugates, the sizes and conjugation efficiency of QD-strep-biotin-IgG conjugates were compared to EDC-mediated QD-IgG conjugates. The results from three DBSPS experiments (Fig. 6) yielded ≈ 30 nm larger R_h for QD-SA-biotin-IgG conjugates compared to un-conjugated streptavidin QD 655 (19.6 ± 9.2 nm), and DBSPS shows that these conjugates are ≈ 17 nm larger than the EDC-mediated IgG conjugates. DBSPS measurements also show that the QD-SA-biotin-IgG conjugation efficiency (61 %) is less then EDC mediated QD-IgG conjugates (88 %). Compared to un-conjugated streptavidin QD 655, our measurements on QD-strep-biotin-IgG at increasing binding ratios of 1:1, 1:2, 1:4 and 1:8 yielded significantly larger R_h values of 52.2 ± 17.6 nm, 51.3 ± 18.2 nm, 51.8 ± 20.5 nm and 50.0 ± 18.7 nm, respectively (Fig. 6A-D, asterisk). These results clearly show that DBSPS distinguishes the size difference between un-conjugated QDs (COOH QD: 11.5 nm and strep QD: 19.6 nm), EDC mediated QD-IgG conjugates (28.8-38.5 nm) and QD-strep-biotin-IgG conjugate (50.0-52.2 nm).

In figure 7, we summarize QD and QD-bioconjugate size measurements obtained from DBSPS. This figure shows that particle size increases with the addition of bioconjugates on top of the QD core. Moreover, it also shows that the hydrodynamic radius of particles are larger then the geometric radius reported in literature.

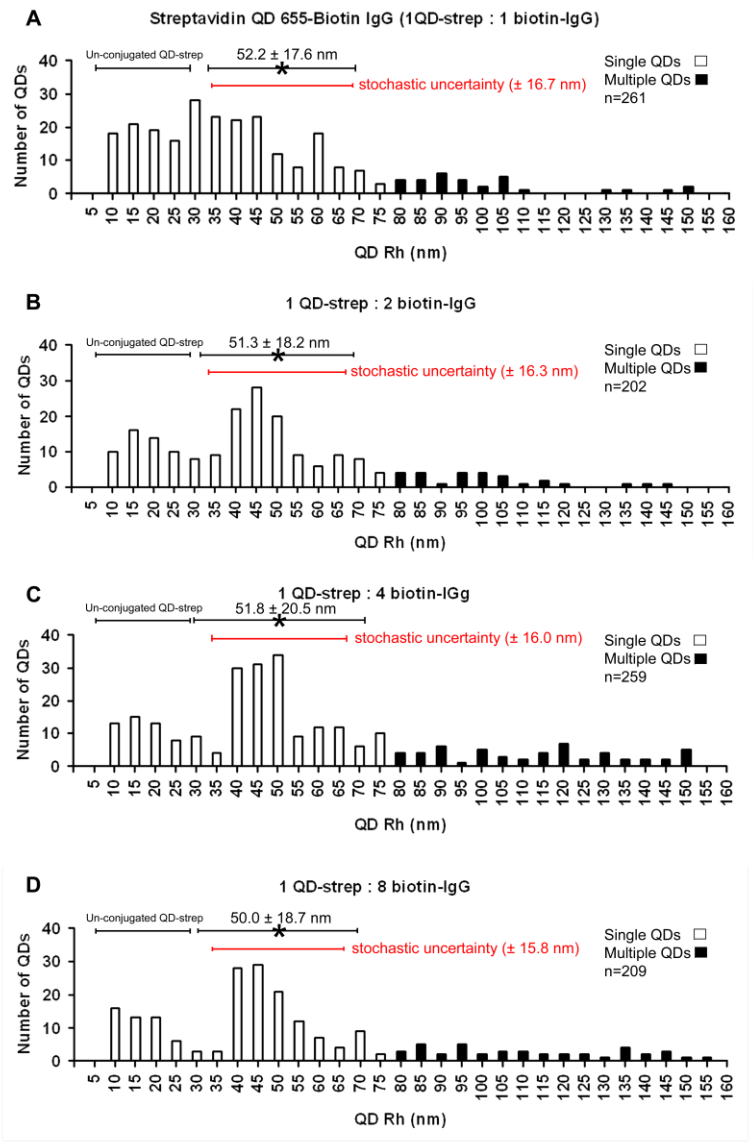

Figure 6. DBSPS measurements showed that QD-strep-biotin-IgG conjugates are larger then both the un-conjugated QD-streps and EDC mediated QD-IgG conjugates. QD-strep-biotin-IgG R_h measurements at increasing binding ratios are as shown. (A-D) 1 QD-strep:1 biotin-IgG, 1 QD-strep:2 biotin-IgG, 1 QD-strep:4 biotin-IgG and 1 QD-strep:8 biotin-IgG binding ratios yielded R_h of (mean ± SD) 52.2 ± 17.6, 51.3 ± 18.2 nm, 51.8 ± 20.5 nm and 50.0 ± 18.7 nm, respectively. In all binding ratios the R_h measurements detect two distinct set of QD R_h, one set at smaller R_h (10-30 nm) and a set at larger R_h (35-75 nm). The smaller set of QDs are un-conjugated QD-streps. DBSPS and QD fluorescence intensity analysis differentiates single QDs (white bars) and multiple QDs (black bars).The Error due to stochastic uncertainty (red horizontal bar) was calculated for all the particle trajectories. Histogram bin size: 5nm

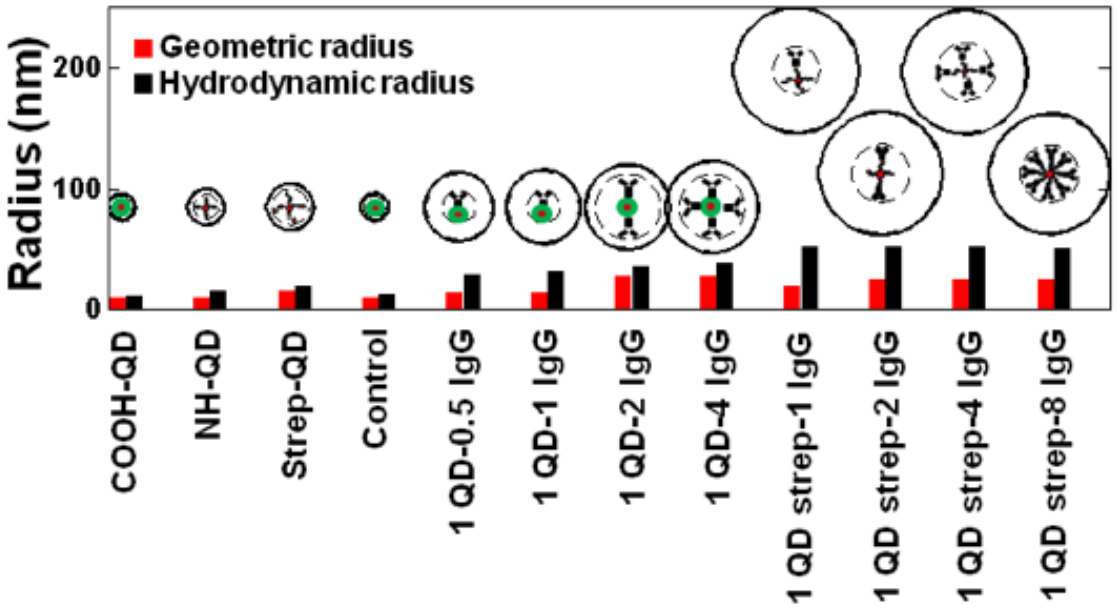

Figure 7. Summary figure comparing the hydrodynamic radius of QDs and QD-bioconjugates measured with DBSPS to the geometric radius reported in literature. –Denotes the inorganic QD core. –Denotes the COOH organic layer on top of the QD core. –Denotes the amino-PEG layer on top of the QD core. –Denotes the streptavidin proteins conjugated to the amino-PEG layer on top of the QD core. –Denotes the IgG conjugation on top of the COOH-QD. –Denotes the IgG-biotin-streptavidin-QD conjugates. Solid circle around the particles denotes the effective hydrodynamic size and dashed circle denotes the geometric size of the particle.

4. Discussion

We have introduced a single-particle fluorescence imaging method that can estimate the hydrodynamic radii of QD bio-conjugates to within few nanometers. As expected, the diffusion coefficient decreases and R_h increases with QD conjugation to bio-molecules. We also confirm, through statistical analysis, that with 9.7 ± 6.6 (n = 3465) particle position measurements, the error is small at the nano-scale (≈ ± 3 nm for 10 nm particles). As a check of the validity of this method, R_h was estimated for both QDs (conjugated to different size bio-molecules) and pre-calibrated polystyrene nanospheres. The experimental results show that the QD conjugates and large pre-calibrated polystyrene nanospheres exhibit a significantly larger R_h compared to un-conjugated QDs and smaller pre-calibrated polystyrene nanospheres. Furthermore, QD R_h measurements (655QD-COOH: 11.5 nm, 655QD-NH: 15.3 nm and 655QD-SA: 19.6 nm) are in the same range as the measurements made by other methods (Gel electophoresis, SEC, PCS, FCS, and ultracentrifugation).[11, 14]

DBSPS has several advantages over other methods. DBSPS takes a single particle sizing approach compared to an ensemble averaging approach taken by Gel electophoresis, SEC, PCS, FCS, ultracentrifugation or thermophoresis.[14, 46] Since each single particle is detected separately, we are able to track and analyze small particles even when they are present in heterogeneous samples containing larger particles. In addition, this method provides the biologically relevant hydrodynamic radii of nano-particles in comparison to TEM which measures the geometric radius of particles missing the layer of water molecules around particle in solution.[9, 16] DBSPS is even more advantageous because of its simplicity compared to other methods, which require more costly optics and instruments. In contrast, DBSPS only requires a florescent microscope with x100 oil immersed magnification and a sufficiently sensitive camera. DBSPS sample preparation is also minimal requiring only dilution in aqueous solution. The number of detected QDs simply depend on the

concentration of the QDs in the aqueous solution (20 pM- 200 pM). Significantly, DBSPS is well suited for QDs because the stochastic uncertainties in R_h measurements translate into an absolute error of only a few nanometers for QDs. This report shows that DBSPS is an attractive alternative or compliment to higher cost and more complex methods of nano-particle analysis.

There are technical limitations to DBSPS. For example, DBSPS is limited to fluorescent particles. QD fluorescence signals are observed in the focal plane of the fluorescent microscope. But the fluorescence signal diminished significantly once QDs moved out of the focal plane. The movement of the QDs out of the focal plane limits the number of particle positions captured (we obtained 9.7 ± 6.6 position measurements with a frame acquisition rate of 31 frames/s), increasing the stochastic uncertainty in R_h estimation. However, this stochastic uncertainty translates into only a few nanometers (≈ ± 3 nm) for nano-particle QDs and it may be further reduced by using the higher temporal resolution of faster cameras (higher frame acquisition rate). Faster cameras capture larger numbers of independent particle positions, reducing the stochastic uncertainty in R_h measurements and increasing DBSPS sensitivity.[35] The particle tracking algorithm must also be good enough to reliably and accurately track the moving particles, otherwise the error introduced by the particle tracker can skew the data significantly. The particle tracking software we used, ImageJ 1.38X (NIH) with the particle tracking plugin (Guy Levy, computational biophysics lab, ETH Zurich), introduces negligible error because it has a tracking accuracy and precision of about 0.2 pixels.[30] Fluctuations in temperature/viscosity is another source of error, but this error (≈ ± 0.7 nm) is small relative to the DBSPS sensitivity (≈ ± 3 nm for 10 nm particles). In addition, shapes of particles that are different from perfect spheres may be a source of error. This source of error is negligible with DBSPS because particles moving in fluids have rotational movements that cause them to form an effective spherical shape.[36-40] Finally, we point out that another group (Suzuto et al. 2007) and a privately owned company (Nanosight Ltd) have recently and independently developed a hydrodynamic size measuring method that employs single particle tracking.[47] Their approach differs

from ours primarily by the method by which the positions of particle are resolved. We use the inherit fluorescence property of the QDs and fluorescent nanospheres for particle detection and the other two methods use laser light scattering by particles for detection. It is important to note that the approach of Suzuto and Nanosight is suitable for all particles large enough to scatter light, rather than only fluorescent particles. The disadvantage, however is that QDs are too small to scatter light efficiently due to the Rayleigh limit[48] and are therefore hard to detect with the Suzuto and Nanosight method.

5. Conclusions

Simple methods for measuring QD and QD bio-conjugate hydrodynamic dimensions are important for designing well-dispersed QD bio-conjugates suited for specific biological settings. We have demonstrated that DBSPS is a robust method to characterize the hydrodynamic dimensions of single hydrophilic QDs. The R_h of series of QD-IgG bio-conjugates using different conjugation schemes (EDC and streptavidin-biotin) were analyzed. We have shown that DBSPS detects significant size increases with IgG conjugation. We further showed that streptavidin-biotin conjugates result in larger conjugates compared to EDC mediated conjugates and EDC mediated conjugation is more efficient then streptavidin-biotin mediated conjugation. We also showed that DBSPS is suited for nano-particles because the relative error from the stochastic uncertainty (≈ ±30%) presents a small absolute error (≈ ± 3 nm for 10 nm particles) at the nano scale. Finally, we assert that this method's simplicity makes it optimal for use in single molecule imaging studies of biomolecules.

6. References

1. Medintz, I. L.; Berti, L.; Pons, T.; Grimes, A. F.; English, D. S.; Alessandrini, A.; Facci, P.; Mattoussi, H. *Nano Lett* **2007,** 7, (6), 1741-8.

2. Gerhards, C.; Schulz-Drost, C.; Sgobba, V.; Guldi, D. M. *J Phys Chem B* **2008**.

3. Howarth, M.; Liu, W.; Puthenveetil, S.; Zheng, Y.; Marshall, L. F.; Schmidt, M. M.; Wittrup, K. D.; Bawendi, M. G.; Ting, A. Y. *Nat Methods* **2008,** 5, (5), 397-9.

4. Yusuf, H.; Kim, W. G.; Lee, D. H.; Guo, Y.; Moffitt, M. G. *Langmuir* **2007,** 23, (2), 868-78.

5. Hermanson, G. T., *Bioconjugate Techniques*. Academic Press: Rockford, Illinois, 1996.

6. Chan, W. C.; Maxwell, D. J.; Gao, X.; Bailey, R. E.; Han, M.; Nie, S. *Curr Opin Biotechnol* **2002,** 13, (1), 40-6.

7. Parak, W. J.; Pellegrino, T.; Micheel, C. M.; Gerion, D.; Williams, S. C.; Alivisatos, A. P. *Nano Lett.* **2003,** 3, (1), 33-36.

8. Pellegrino, T.; Sperling, R. A.; Alivisatos, A. P.; Parak, W. J. *J Biomed Biotechnol* **2007,** 2007, 26796.

9. Nehilla, B. J.; Vu, T. Q.; Desai, T. A. *J Phys Chem B* **2005,** 109, (44), 20724-30.

10. Calabretta, M.; Jamison, J. A.; Falkner, J. C.; Liu, Y.; Yuhas, B. D.; Matthews, K. S.; Colvin, V. L. *Nano Letters* **2005,** 5, (5), 963-967.

11. Lees, E. E.; Gunzburg, M. J.; Nguyen, T. L.; Howlett, G. J.; Rothacker, J.; Nice, E. C.; Clayton, A. H.; Mulvaney, P. *Nano Lett* **2008,** 8, (9), 2883-90.

12. Moris, S. B., H. G. , *Size Exclusion Chromatography*. Springer: New York, 1999.

13. Hagel, L., *Gel Filtration. In Protien Purification. Principles, High Resolution Methods and Applications*. John Wiley & Sons: New York, 1998.

14. Sperling, R. A.; Liedl, T.; Duhr, S.; Kudera, S.; Zanella, M.; Lin, C. A. J.; Chang, W. H.; Braun, D.; Parak, W. J. *J. Phys. Chem. C* **2007,** 111, (31), 11552-11559.

15. Pecora, R., *Dynamic Light Scattering: Applications of Photon Correlation Spectroscopy*. Springer: New York, NY, 1985.

16. Pons, T.; Uyeda, H. T.; Medintz, I. L.; Mattoussi, H. *J Phys Chem B* **2006,** 110, (41), 20308-16.

17. W. M. Deen, M. P. B. N. B. E. *AIChE Journal* **1981,** 27, (6), 952-959.

18. Salmeen, I.; Rimai, L.; Luftig, R. B.; Libes, L.; Retzel, E.; Rich, M.; McCormick, J. J. *J Virol* **1976,** 17, (2), 584-96.

19. Geerts, H.; De Brabander, M.; Nuydens, R.; Geuens, S.; Moeremans, M.; De Mey, J.; Hollenbeck, P. *Biophys J* **1987,** 52, (5), 775-82.

20. Ross, D.; Dimas, N. *Particle & particle systems characterization* **1993,** vol. 10, (no2), 62-69

21. Dembo, M.; Harris, A. K. *J Cell Biol* **1981,** 91, (2 Pt 1), 528-36.

22. Clarke, S. J.; Hollmann, C. A.; Aldaye, F. A.; Nadeau, J. L. *Bioconjug Chem* **2008,** 19, (2), 562-8.

23. Xing, Y.; Chaudry, Q.; Shen, C.; Kong, K. Y.; Zhau, H. E.; Chung, L. W.; Petros, J. A.; O'Regan, R. M.; Yezhelyev, M. V.; Simons, J. W.; Wang, M. D.; Nie, S. *Nat Protoc* **2007,** 2, (5), 1152-65.

24. Nakamura, M.; Tsumoto, K.; Ishimura, K.; Kumagai, I. *Analytical Biochemistry* **2002,** 304, (2), 231-235.

25. Wilchek, M.; Bayer, E. A. *Trends Biochem Sci* **1989,** 14, (10), 408-12.

26. Wilchek, M.; Bayer, E. A. *Methods Enzymol* **1990,** 184, 5-13.

27. Gelles, J.; Schnapp, B. J.; Sheetz, M. P. *Nature* **1988,** 331, (6155), 450-453.

28. Azizi, F.; Wahl, P. *Biochimica et Biophysica Acta (BBA) - Biomembranes* **1997,** 1327, (1), 75-88.

29. De Brabander, M.; Nuydens, R.; Geerts, H.; Hopkins, C. R. *Cell Motil Cytoskeleton* **1988,** 9, (1), 30-47.

30. Sbalzarini, I. F.; Koumoutsakos, P. *J Struct Biol* **2005,** 151, (2), 182-95.

31. Sonesson, A. W.; Elofsson, U. M.; Callisen, T. H.; Brismar, H. *Langmuir* **2007,** 23, (16), 8352-6.

32. Schmidt, T.; Schutz, G. J.; Baumgartner, W.; Gruber, H. J.; Schindler, H. *Proc Natl Acad Sci U S A* **1996,** 93, (7), 2926-9.

33. Sheetz, M. P.; Steuer, E. R.; Schroer, T. A. *Trends Neurosci* **1989,** 12, (11), 474-8.

34. Saxton, M. J. *Biophys J* **1997,** 72, (4), 1744-53.

35. Qian, H.; Sheetz, M. P.; Elson, E. L. *Biophys J* **1991,** 60, (4), 910-21.

36. Nichols, F. A. *Journal of Materials Science* **1976,** 11, (Number 6 / June, 1976), 1077-1082.

37. Lee, N. K.; Johner, A.; Thalmann, F.; Cohen-Tannoudji, L.; Bertrand, E.; Baudry, J.; Bibette, J.; Marques, C. M. *Langmuir* **2008,** 24, (4), 1296-307.

38. Borejdo, J.; Putnam, S.; Morales, M. F. *Proc Natl Acad Sci U S A* **1979,** 76, (12), 6346-50.

39. Kask, P.; Piksarv, P.; Mets, U.; Pooga, M.; Lippmaa, E. *Eur Biophys J* **1987,** 14, (4), 257-61.

40. Cummins, H. Z.; Carlson, F. D.; Herbert, T. J.; Woods, G. *Biophys J* **1969,** 9, (4), 518-46.

41. Clapp, A. R.; Goldman, E. R.; Mattoussi, H. *Nat. Protocols* **2006,** 1, (3), 1258-1266.

42. Saxton, M. J. *Biophys J* **1994,** 66, (2 Pt 1), 394-401.

43. Saxton, M. J.; Jacobson, K. *Annu Rev Biophys Biomol Struct* **1997,** 26, 373-99.

44. Gritti, F.; Guiochon, G. *J Chromatogr A* **2008,** 1212, (1-2), 35-40.

45. Nan, X.; Sims, P. A.; Chen, P.; Xie, X. S. *J Phys Chem B* **2005,** 109, (51), 24220-4.

46. Ipe, B. I.; Shukla, A.; Lu, H.; Zou, B.; Rehage, H.; Niemeyer, C. M. *Chemphyschem* **2006,** 7, (5), 1112-8.

47. Suzuto, M.; Nakamura, A.; Yamanishi, Y.; Suzaki, E.; Kataoka, K.; Masujima, T. *Nanomed* **2007,** 2, (1), 63-70.

48. Huffman., C. F. B. a. D. R., *Absorption and scattering of light by small particles*. John Wiley & Sons: New York, 1983.

49. Bicknell G.V., The equations of motion of particles in smoothed particle hydrodynamic, SIAM J. Stat. **1991,**12, 1198-1206.